Engineering Fracture Mechanics, Volume 76, Issue 11, July 2009, Pages 1589-1602

Predicting fatigue crack growth rate in a welded butt joint: the role of effective *R* ratio in accounting for residual stress effect

G. Servetti, X. Zhang

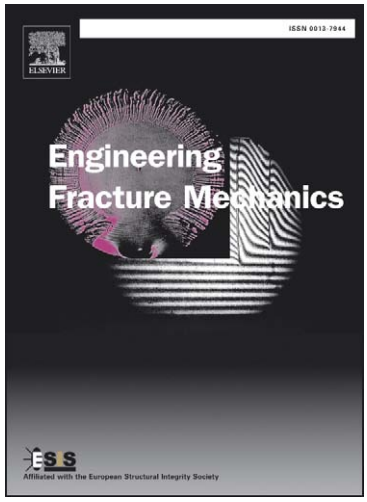

PII: S0013-7944(09)00065-4
DOI: 10.1016/j.engfracmech.2009.02.015
Reference: EFM 2977

To appear in: *Engineering Fracture Mechanics*

Received Date: 15 August 2008
Revised Date: 4 February 2009
Accepted Date: 16 February 2009

Please cite this article as: Servetti, G., Zhang, X., Predicting fatigue crack growth rate in a welded butt joint: the role of effective *R* ratio in accounting for residual stress effect, *Engineering Fracture Mechanics* (2009), doi: 10.1016/j.engfracmech.2009.02.015

Predicting fatigue crack growth rate in a welded butt joint: the role of effective *R* ratio in accounting for residual stress effect

G. Servetti, X. Zhang*

Department of Aerospace Engineering, School of Engineering, Cranfield University

Bedford, MK43 0AL, U.K.

Abstract: A simple and efficient method is presented in this paper for predicting fatigue crack growth rate in welded butt joints. Three well known empirical crack growth laws are employed using the material constants that were obtained from the base material coupon tests. Based on the superposition rule of the linear elastic fracture mechanics, welding residual stress effect is accounted for by replacing the nominal stress ratio (R) in the empirical laws by the effective stress intensity factor ratio (R_{eff}). The key part of the analysis process is to calculate the stress intensity factor due to the initial residual stress field and also the stress relaxation and redistribution due to crack growth. The finite element method in conjunction with the modified virtual crack closure technique was used for this analysis. Fatigue crack growth rates were then calculated by the empirical laws and comparisons were made among these predictions as well as against published experimental tests, which were conducted under either constant amplitude load or constant stress intensity factor range. Test samples were M(T) geometry made of aluminium alloy 2024-T351 with a longitudinal weld by the variable polarity plasma arc welding process. Good agreement was achieved.

Keywords: Weld joint; thermal residual stress; fatigue crack growth rate; finite element method; virtual crack closure technique; mutual work.

Nomenclature

a	Half of the crack length
E	Young's modulus
F_{app}, F_{res}, F_{tot}	Reaction force at crack-tip node due to applied, residual and combined (total) stresses
G_{app}, G_{res}, G_{tot}	Strain energy release rates due to applied, residual and combined (total) stress fields
K_{app}, K_{res}, K_{tot}	Stress intensity factors (SIF) due to applied, residual and combined stress fields
$K_{app,max}$, $K_{tot,max}$	SIF due to applied and combined stress fields at the maximum applied stress
$K_{app,min}$, $K_{tot,min}$	SIF due to applied and combined stress fields at the minimum applied stress

* Corresponding author. Tel.: +44 1234 754621; fax: +44 1234 758203.
Email address: xiang.zhang@cranfield.ac.uk (X. Zhang)

K_C	Apparent fracture toughness
R	Nominal stress intensity factor ratio ($K_{min}/K_{max} = \sigma_{min}/\sigma_{max}$)
R_{eff}	Effective stress intensity factor ratio ($K_{tot,\,min}/K_{tot,\,max}$)
v_{app}, v_{res}, v_{tot}	Crack opening displacements due to applied, residual and combined (total) stresses
β	Non-dimensional SIF
ΔK_{app}, ΔK_{tot}	SIF range due to applied and combined applied and residual stresses
C, n, m, p, q	Material constants in the various crack growth laws

1. Introduction

In the last decade trends in aircraft manufacture are towards creation of integral structures via manufacturing processes such as welding, casting and forging, high-speed machining, rather than the traditional riveting [1-2]. This is mainly driven by manufacture cost saving and structural weight reduction for the future aircraft structures. Current welding processes applicable to airframe aluminium alloys include the friction stir welding (FSW), laser beam welding (LBW), and plasma arc welding, e.g. the variable polarity plasma arc (VPPA) and metal inert gas (MIG) welding. One of the main advantages of welded structures is the significant reduction or complete removal of the numerous fasteners and overlapping joint areas in the airframe; this will bring down the costs of manufacture and maintenance significantly, and also the structural weight. The absence of fastener holes will also remove the crack initiation sources resulting in much improved fatigue endurance and simplification in inspection.

Welding also produces adverse effects on fatigue crack growth (FCG) rate due to thermal residual stresses, local distortions (especially in thin alloy sheets) and the microstructure and hardness changes in the heat-affected zones (HAZ). Whereas all of these affect the FCG rates, thermal residual stress has been identified as the most influential factor, and this was demonstrated in the friction stir welds [3-4] and plasma welds [5]. Efforts have been devoted to the investigation of residual stress effect on FCG rates [e.g. 3-14].

Two methods have been widely used to calculate FCG rates in residual stress fields. One employs the superposition rule to determine the effective stress ratio (R_{eff}) to account for the residuals stress effect [7-8]. The other is based on the crack closure concept originally proposed by Elber [15] by calculating the crack opening stress intensity factor (K_{open}) and then the effective stress intensity factor range (ΔK_{eff}) in a combined stress field of the applied and residual. The validity of both methods has been generally accepted. For the second approach, some researchers calculate K_{open} by empirical formulas [8-10], whereas others by the finite element method [11, 13].

The key task for the first method is to determine the K_{res} using either the weight function method (WFM) or the finite element method (FEM). The WFM has been successfully used by several researchers, e.g. [7, 14, 16], for simple geometries. FEM is more powerful and robust when general SIF solutions cannot be found due to the complexity in either geometry or loading conditions. The subsequent task is to calculate the FCG rates by empirical laws. The most frequently used are in the form of $da/dN = f(\Delta K, R)$. The Walker [17], Hater T-method [18], and NASGRO equation [18] all belong to this category. Another method is the so-called alternate superposition approach, in which $K_{tot,max}$ and $K_{tot,min}$ are calculated at the cyclic maximum and minimum stresses and then find the range ΔK_{tot}. Negative $K_{tot,min}$ value is set to zero [e.g. 8, 19-20]. A two-parameter rule was also proposed to take account of the K_{max} contribution in the form of $da/dN = f(\Delta K, K_{max})$ [21-22].

The objective of this paper is to present a simple method for predicting FCG rate using the base material coupon test data and the effective stress ratio to account for the residual stress effect. FEM was used for calculating the SIF due to the applied and residual stress fields. The Walker, Harter T-method and NASGRO equation were employed for calculating the FCG rate. The predicted results were validated by test data of an M(T) specimen with a longitudinal VPPA weld for two load cases: constant amplitude loads for R ratios of 0.1 and

0.6 and constant stress intensity factor ranges. The purpose is to demonstrate that if the base material FCG rates are measured for two different nominal *R* ratios, then FCG rates of welded panels can be predicted by these empirical laws using the effective stress ratio to account for the welding residual stress effect.

During the course of this research we have also found a computational issue that is worth reporting, that is, if the total strain energy release rate due to the applied and residual stresses is calculated by two separate FE analyses under the respective applied stress fields, then the mutual work due to the interactions of the two stress fields must be counted in the total strain energy term. This is demonstrated in an example in this paper.

2. FE modelling approach

2.1 Specimen and material properties

Test sample in [12, 13] was used in this study that is a middle-crack tension, M(T), geometry made of aluminium alloy 2024-T351. The sample contains a longitudinal weld by single pass autogenous variable polarity plasma arc (VPPA) welding process. Dimensions and weld orientation are shown in Fig. 1. Base material properties are E = 73 GPa, yield and ultimate tensile strengths 372 and 470 MPa, respectively.

2.2 Inputting initial residual stress field into FE model

In [5, 13], the neutron diffraction technique was used to measure the welding residual strains in the longitudinal, transverse and normal directions, which were subsequently converted to the corresponding residual stresses in all three directions. This initial residual stress filed is self-balanced and exists before any external mechanical loads being applied to the specimen and prior to the introduction of an initial crack.

Many researchers have developed methods to input residual stresses into the FE models [e.g. 13]. In this study two approaches were adopted, i.e. inputting equivalent initial displacements and inputting measured residual stresses. In the first method, initial displacements were

determined from measured residual strains in both the longitudinal and transverse directions. These displacements were then inputted into the FE model as an initial condition by a subroutine interfacing the ABAQUS code. From these initially applied displacements a distribution of residual stresses is imposed to the FE model. In the second method, measured residual stress distribution was inputted into the FE model using an ABAQUS subroutine named SIGINI. After inputting the stresses, ABAQUS command "UNBALANCED STRESSES" was called to balance the inputted stresses to satisfy the equilibrium condition. It is also necessary to relax the stresses under the equilibrium condition to make the stress-free condition at the free edges. Without external loads, the specimen is self-balanced under the initial residual stress filed.

The inputted residual stresses by both methods are shown in Fig. 2, which are in good agreement with the measured data published in [13]. Directly inputting residual stresses matches the experimental data better than inputting equivalent initial displacements. Since each node must be constrained for the displacement input method, this method cannot be used to model residual stress re-distribution during crack growth. The stress input method is a better approach because the condition of the virtual work principle is satisfied and the evolution of the residual stresses due to crack extension can be modelled.

2.3 Modelling crack extension under static load and residual stress redistribution

Analyses were performed by 2D FE models using the commercial code ABAQUS (standard version 6.6) [23]. Quadrilateral 4-node shell elements with reduced integration were used and plane stress condition was assumed. The mesh size near the crack tip region and along the crack growth path was 0.5 x 0.5 mm. Because of the geometrical symmetry only a quarter of the plate was modelled. For each crack length, SIF was calculated at the applied stress level followed by releasing the crack-tip node to the next crack length. This process was repeated

for the crack length range from the initial to the final crack size. Therefore, residual stress redistribution due to crack extension was modelled.

Fig. 3 shows the redistribution of residual stresses for different crack lengths and comparison with measured data in [13]. Since the FE analysis was linear elastic, there is a peak in the calculated stress distribution near the crack tip position that is much higher than the measured value due to the stress singularity effect and such peak stress is dependent on the FE mesh size. In this very small crack tip zone comparison with the experimental data is poor. However, away from the crack tip region the calculated residual stress distribution due to crack extension agrees with the measured. The discrepancy in the crack-tip stress values should not affect the fracture mechanics analysis conducted in this study, since the SIF was calculated indirectly from the strain energy release rate.

2.4 Calculating K_{app}, K_{res} and K_{tot}

1) MVCCT approach

The modified virtual crack closure technique known as the MVCCT or VCCT method [24] was used for calculating the strain energy release rate (SERR or G) due to crack extension:

$$G = \frac{1}{2t\Delta a} F_{yy,i}(v_j - v_j^*) \qquad (1)$$

where $F_{yy,i}$ is the nodal reaction force perpendicular to the crack growth path at the crack tip node i, $(v_j - v_j^*)$ the crack opening displacement at node j immediately behind the crack tip as shown in Fig. 4, Δa the crack extension length that equals to the crack tip element size, and t the plate thickness.

Stress intensity factor (SIF or K) can be found by:

$$K = \sqrt{GE} \text{ (plane stress)} \qquad K = \sqrt{\frac{GE}{1-\upsilon^2}} \text{ (plane strain)} \qquad (2)$$

The relation between K and G only holds for the linear elastic material behaviour. Since the VCCT is an energy-based method, calculated G and K values are less dependent on the finite element mesh size.

2) The total SIF (K_{tot})

Superposition has been widely used in the framework of LEFM, especially when the weight function method is employed to estimate the K_{res}. Two separate analyses are necessary to find the K_{app} and K_{res} and then the K_{tot}:

$$K_{tot} = K_{app} + K_{res} \tag{3}$$

The calculations of strain energy release rate and SIF described in eqs. (1) & (2) can be performed separately for both externally applied and internal residual stress fields. As illustrated in Fig. 5, by applying the respective stress field to the same FE model, G_{app} and G_{res} can be found by eq. (1) and then K_{app} and K_{res} be calculated by eq. (2) for the respective stress fields.

Fig. 6 shows the calculated K_{res} by FEM and the initial residual stress distribution for the case given in section 2.1. The horizontal axis is the half crack length that is also the distance from the weld centre. Since the plate was subjected to the initial residual stress field only, the calculated K_{res} follows the same trend of the initial residual stress distribution.

An alternative approach to calculate the K_{tot} is to subject the FE model to a combined stress field of the applied and residual stresses. G_{tot} can be found by eq. (1) with $F_{yy,i}$ and $(v_j - v_j^*)$ representing the crack-tip force and crack opening displacement under the combined stress filed. K_{tot} can then be found by:

$$K_{tot} = \sqrt{G_{tot} E} \text{ (plane stress)} \quad K_{tot} = \sqrt{\frac{G_{tot} E}{1 - \upsilon^2}} \text{ (plane strain)} \tag{4}$$

Only one FE analysis is needed. Calculated K_{tot} by eq. (3) and (4) have been validated against published work; both equations give the same result.

Whereas superposition of stress intensity factors has been widely used, especially when K_{res} is calculated by the WFM, it should be pointed out that simply summing the two strain energy release rate terms, G_{app} and G_{res}, will not deliver the correct value of G_{tot}. The work done by the externally applied stress interacts with the work done by the internal residual stresses, and vice versa. Therefore, the mutual work done by the reaction forces due to applied stress (F_{app}) over the displacement caused by the residual stresses (v_{res}) should be counted, and vice versa (Figs. 5a & 5b). From the MVCCT formula the total strain energy release rate (G_{tot}) should also contain the mutual work term:

$$G_{tot} = \frac{1}{2t\Delta a}(F_{app} + F_{res}) \cdot (v_{app} + v_{res}) \tag{5}$$

$$G_{tot} = \frac{1}{2t\Delta a}(F_{app}v_{app} + F_{res}v_{res} + F_{app}v_{res} + F_{res}v_{app}) = G_{app} + G_{res} + G_{mut} \tag{6}$$

where, the mutual work term is expressed as:

$$G_{mut} = \frac{1}{2t\Delta a}(F_{app}v_{res} + F_{res}v_{app}) \tag{7}$$

If one attempts to find G_{tot} by conducting two separate FE analyses to find G_{app} and G_{res} and to simply sum them, then the mutual work contribution is lost. This can be demonstrated by Fig. 7, where the superposition of K ($K_{tot} = K_{app} + K_{res}$) is plotted in Fig. 7a and superposition of G with and without the mutual work in Fig. 7b. Calculations to obtain K_{tot} are performed by either superposition using eq. (3) or via computing the total strain energy release rate by eq. (4); K_{tot} values determined by both methods are identical. Mathematical deductions of the mutual work are given in Appendix A.

It is important to point out that this does not contradict to the mixed mode fracture problems, where contribution to the G_{tot} from the SERR of three different load modes (G_I, G_{II} and G_{III}) are additive because SERR is a scalar quantity [25]. In this case, the mutual work terms are calculated from the crack-tip force and displacement caused by two different loading modes, e.g. force caused by the mode I load and displacement by mode II load. Since the force and

displacement are orthogonal to each other, the product of them is zero, i.e. no mutual work is done. In the case presented in this paper the mutual energy terms are not orthogonal (both are in mode I). However, when thermal residual stresses or secondary bending occur in the mixed mode problems, the mutual work between those loads must be considered.

3. Predicting fatigue crack growth rates

Glinka [6] and Parker [7] originally proposed the superposition method based on the principle of linear elastic fracture mechanics (LEFM). Under the cyclic loads, the total SIF range (ΔK_{tot}) and effective SIF ratio (R_{eff}) are calculated as:

$$\Delta K_{tot} = (K_{app,\max} + K_{res}) - (K_{app,\min} + K_{res}) = \Delta K_{app} \tag{8}$$

$$R_{eff} = (K_{app,\min} + K_{res}) / (K_{app,\max} + K_{res}) \tag{9}$$

Therefore under cyclic loads, only the R_{eff} changes due to the presence of residual stresses. It's worth noting that R_{eff} is the crack tip stress ratio based on the calculated values of $K_{tot,max}$ and $K_{tot,min}$, hence R_{eff} is not the same as the nominal applied stress ratio (R). The Walker [17], Harter T-method [18], and NASGRO [18] equations were used to calculate FCG rates using R_{eff} to replace the nominal R ratio in the original equations.

Original Walker equation is expressed as:

$$\frac{da}{dN} = C(\Delta K_{app}(1-R)^{(m-1)})^n \tag{10}$$

Where C and n are the coefficients of the Paris law, m a constant that can be found from test data conducted at two different nominal stress ratios (R_1 and R_2):

$$m = 1 + \left[\log\left(\frac{\Delta K_1}{\Delta K_2}\right) / \log\left(\frac{(1-R_2)}{(1-R_1)}\right) \right] \text{ for } R_1 \geq 0, R_2 \geq 0 \tag{11}$$

The value of m is controlling the shift of the crack growth rate curves for different R ratios and it depends on the material properties.

Considering the welding residual stress effect the Walker equation is expressed as:

$$\frac{da}{dN} = C(\Delta K_{app}(1-R_{eff})^{(m-1)})^n \tag{12}$$

Substitute R_{eff} by eq. (9), we get:

$$\frac{da}{dN} = C(\Delta K_{app}(\frac{\Delta K_{app}}{K_{app,\max}+K_{res}})^{(m-1)})^n \tag{13}$$

which means that the FCG rate depends upon three parameters, ΔK_{app}, K_{res} and $K_{app,max}$.

The Harter T-Method refers to the original "Point-by-Point Walker Shift Method" proposed by Harter as a means to interpolate and/or extrapolate crack growth rate data using a limited amount of tabular crack growth rate test data. The AFGROW code uses the Walker equation on a point-by-point basis (Harter T-Method) to determine crack growth rate shifting as a function of the stress ratio [18].

Considering the welding residual stress effect the original NASGRO equation is expressed as:

$$\frac{da}{dN} = C\left[\left(\frac{1-f}{1-R_{eff}}\right)\Delta K_{app}\right]^n \frac{\left(1-\frac{\Delta K_{th}}{\Delta K_{app}}\right)^p}{\left(1-\frac{K_{app,\max}+K_{res}}{K_{crit}}\right)^q} \tag{14}$$

4. Validation of prediction method

Predicted FCG rates were compared with test results for an M(T) specimen made of aluminium alloy 2024-T351 welded by the VPPA process as described in Section 2.1. Two cases were considered: constant amplitude loads with two different R ratios and constant ΔK_{app}. Experimental results are taken from [12-13]. The Walker, Harter T-method, and NASGRO equation were employed to calculate the crack growth rates. Material constants used in the Walker and NASGRO equations were found from the NASGRO database [26] and listed in Table 1.

4.1 Constant amplitude load

Fig. 8a shows the predicted FCG rates for the R = 0.1 case at constant applied stress range of 46.35 MPa. For comparison the base material growth rate is also shown which was calculated by the NASGRO equation. For the welded joint, both NASGRO and Harter T-method give good predictions with typical error range of ±5% compared to the measured. Walker equation underestimates the FCG rate considerably when half crack length (a) is larger than 17 mm with an error range of 15-30%.

Fig. 8b shows the R = 0.6 case with applied stress range of 42.6 MPa. For this test, the Harter T-method and NASGRO give good predictions. Walker equation gives good prediction when a < 17 mm. It should be noted that in the measured crack growth rate curve there is a sudden change of the curve trend from a convex to concave within the crack length of 7.5 to 11.5 mm, whereas the predicted curves are generally in a convex shape. The base material growth rate is also shown that is very close to the measured growth rates for the welded sample. The case is further discussed in Section 5.

4.2 Constant SIF range

In this case crack growth test was conducted by keeping the SIF range (ΔK_{app}) constant. Nominal stress ratio R = 0.1 was maintained throughout the test. According to the Paris law, FCG rate for the base material will remain constant for different crack lengths. However, crack growth rate in the welded sample will change along the distance from the weld centre due to the presence of the welding residual stresses. For constant ΔK_{app}, following set of equations can be deduced:

$$\Delta K_{app} = (\sigma_{\max} - \sigma_{\min})\beta\sqrt{\pi a} = \text{constant} \tag{15}$$

Since a constant R ratio was maintained during the test, the maximum and minimum applied stresses and respective stress intensity factors are functions of the crack length:

$$\sigma_{\max}(a) = \frac{\Delta K_{app}}{(1-R)\beta(a)\sqrt{\pi a}} \quad \text{and} \quad c_{\min}(a) = Rc_{\max} \tag{16}$$

$$K_{app,\max} = \sigma_{\max}\beta\sqrt{\pi a} = \frac{\Delta K}{1-R} \text{ and } K_{app,\min} = \sigma_{\min}\beta\sqrt{\pi a} = \frac{R\Delta K}{1-R} \quad (17)$$

$$R_{eff} = \frac{K_{app,\min} + K_{res}}{K_{app,\max} + K_{res}} \quad (18)$$

In the FCG life prediction analysis, ΔK_{app} (a constant) and R_{eff} are used to replace the ΔK and R in the original Walker, Harter T-method, and NASGRO equations.

Experimental test results were reported in [12] for ΔK_{app} = 4, 6, 11 and 15 MPa√m. Good agreement with the test results is achieved for the lower SIF ranges (ΔK_{app} = 4, 6). However, for higher SIF range (ΔK_{app} = 11, 15), the agreement is not so good. Examples showing the comparison with the tests are presented in Fig. 9 for ΔK_{app} = 6 and 11 MPa√m. For both cases, crack growth rates of the welded sample were significantly higher than that of the base material due to the presence of tensile residual stresses. Overall the NASGRO equation gives better prediction comparing to the Walker equation predicted results.

5. Discussion

5.1 Using R_{eff} in empirical crack growth laws

In this work welding residual stress effect was accounted for by replacing the nominal R ratio with the effective ratio R_{eff}, which is a function of the K_{res} that can be determined by either the FEM or the WFM. With this R_{eff}, three well-known empirical laws were tested.

Walker equation has an appealing advantage for predicting FCG rates in residual stress fields. All one needs to have is a set of measured *da/dN* data for two different R ratios for the base material. The limitation of the Walker equation is that it is too simplistic and it underestimates the final part of the FCG rates when the SIF approaches the material fracture toughness. NASGRO has considered the effect of plasticity induced crack closure by an empirical constant *f*. Although the crack closure effect on *da/dN* can be accounted for by the R ratio to a

certain extent, further correlation of *da/dN* with another parameter should yield more accurate prediction as demonstrated in the results in Figs. 8 and 9. NASGRO equation also takes account of the final fast crack growth stage when K_{max} approaches K_{crit}.

The NASGRO and Harter T-method account for the stress ratio effect more comprehensively compared to the Walker. In NASGRO the factor *f* is a direct function of the stress ratio and in Harter T-method stress ratio is considered by means of point-to-point shift from available test data. Walker equation predicts much slower crack growth rate compared to the other two methods. For materials where the NASGRO equation coefficients are unknown, the Harter T-method (which is a modified version of the Walker equation) can be a good prediction tool.

5.2 Constant amplitude load case

NASGRO equation gives the best prediction of FCG rates for both *R* ratios due to the fact that it has more material "fitting" constants and also takes account of the fast crack growth regime when $K_{max,tot}$ approaches the fracture toughness K_{crit}. Fig. 8 shows that difference between the NASGRO and Walker predictions began to widen when $a > 17$ mm. For crack lengths 17–20 mm, $K_{max,tot}$ is in the range of 41–57 $MPam^{1/2}$. This is close to the fracture toughness of this alloy, which is about 65 $MPam^{1/2}$ (thickness 7 mm).

To further explore the influence of welding residual stresses, measured crack growth rates presented in Figs. 8a & 8b for two different *R* ratios are plotted together in Fig. 10. The closeness of the two test results for two very different nominal *R* ratios may be explained by the crack closure concept originally proposed by Elber [15]. It is now widely accepted that different *da/dN* vs. ΔK_{app} curves for different *R* ratios can be correlated to a single curve by using the effective stress intensity factor range ΔK_{eff} [15, 27-28]. For 2024-T3, Elber proposed following correlation [15]:

$$U = \frac{\Delta\sigma_{eff}}{\Delta\sigma_{app}} = \frac{\Delta K_{eff}}{\Delta K_{app}} = 0.5 + 0.4R \qquad (R > 0) \tag{19}$$

Based on test data of wider range of R ratios, Schijve proposed an improved formula for 2024-T3 sheet material [27]:

$$U = \frac{\Delta\sigma_{eff}}{\Delta\sigma_{app}} = \frac{\Delta K_{eff}}{\Delta K_{app}} = 0.55 + 0.33R + 0.12R^2 \quad (-1.0<R<0.54) \qquad (20)$$

Both equations give close U values for $R > 0$; hence eq. 19 is used in the following analysis for demonstration purpose.

Calculated R_{eff} as function of crack length (which is also the distance from the weld centre) are plotted in Fig. 11. For R = 0.1, R_{eff} is very close to 0.65–0.7 around the weld centre and quickly decreases to 0.5 away from the weld centre; these R_{eff} values are much higher than the nominal R ratio. For R = 0.6, R_{eff} is close to 0.75–0.8 around the weld centre and decreases to 0.7 away from the weld centre. R_{eff} values across the sample width are only moderately higher than the nominal R ratio of 0.6.

Using these R_{eff} to replace the nominal R in eq. (19), factor U and ΔK_{eff} for the welded sample are calculated; ΔK_{eff} is the closure-free SIF range that is the effective crack growth driving force. Calculated ΔK_{eff} values as function of the crack length are presented in Table 2 for the two test cases. It is interesting to observe that, the two different test cases (R = 0.1, 0.6) have virtually the same ΔK_{eff} values resulting in very close crack growth rates as shown in Fig. 10.

In summary, tensile residual stresses (acting like a mean stress) reduce crack closure effect and increase crack growth rates. This effect is most pronounced for lower nominal R ratios. For higher R ratios, the influence of K_{res} on crack growth rates is small. This observation was previously made by authors in [12].

5.3 Constant SIF range cases

The base material FCG rate is a constant under constant SIF range; hence the difference between the FCG rates of the welded and base metal is mainly due to the influence of welding residual stresses, which are accounted for by the R_{eff}. In this study, longitudinal welding

residual stresses around the weld centre are high tensile stresses in the range of 100-150 MPa. Therefore K_{res} and R_{eff} are raised significantly. Fig. 12 shows the calculated R_{eff} values for the constant ΔK_{app} tests manifesting that R_{eff} is much higher for the lower ΔK_{app} values. For ΔK_{app} = 4 and 6 MPa√m, R_{eff} = 0.6–0.86, hence there was almost no crack closure effect and the life prediction should be more accurate.

Both the measured and predicted FCG rate trends follow the variation of K_{res} (Fig. 6), which is lower at the fusion boundary (a = 5 mm) and at its peak at a = 17 mm. Walker and NASGRO predictions agree well with the tests of lower ΔK_{app} (6 MPa√m). However, predictions are not consistent for the higher ΔK_{app} (11 MPa√m), in which Walker equation gives better prediction for a < 15 mm.

Changes in the microhardness and microstructures in the fusion and heat-affected zones will affect the mechanical properties in these zones and hence likely to affect the crack growth rates. This effect cannot be quantified by this present model and this may have affected prediction accuracy in the crack length range of a = 7 – 15 mm (Fig. 9).

6. Conclusions

An analysis procedure is presented for predicting FCG rate in welded longitudinal butt joints. Welding residual stress effect is accounted for by the effective crack tip stress ratio, which is used in empirical crack growth laws. Comparisons are made with measured crack growth rates in a VPPA weld of 2024-T351 alloy subjected to constant amplitude load and constant SIF range.

For the constant amplitude load case, the Walker, Harter T-method and NASGRO equations all give acceptable predictions if the $K_{max,tot}$ is well below the material fracture toughness. NASGRO gives best prediction for the entire crack length range.

For the constant SIF range cases, predictions are mainly affected by the effective R ratio that has larger influence on lower applied SIF ranges.

In terms of calculation techniques, inputting initial residual stresses into an FE model and modelling residual stress redistribution with crack growth can be performed by the ABAQUS software package. Only the base material crack growth rate data and welding residual stresses are required in the analysis. Mutual work due to the interactions of the applied and residual stress fields must be counted if the total strain energy release rate is determined from two separate FE analyses.

The proposed method can be generally employed when crack initiates within a weld and initially in tensile residual stress field. This prediction method should work for those materials and welding processes, in which fatigue crack growth rates are mainly affected by welding induced thermal residual stresses and the influence of hardness and microstructure changes in the heat affected zones can be neglected. This approach has not been assessed for crack initiation and growth in a compressive residual stress field or crack growth towards a weld, nor has it been validated for variable amplitude loads.

Acknowledgement

The authors are grateful to the financial support by the European Union through the Sixth Framework Programme (FP6). The project title is "cost effective integral metallic structures (COINS)".

Appendix A. Mutual work in calculating the total strain energy release rate

When an FE model is subject to both externally applied and thermal residual stresses, a total reaction force yields at each element nodal point that is the sum of the two reaction nodal forces if the loads were applied separately:

$$F_{tot} = F_{app} + F_{res} \tag{A1}$$

The corresponding FE nodal displacements are:

$$v_{tot} = v_{app} + v_{tred} \tag{A2}$$

To determine the mutual work in the strain energy release rate calculation, the starting point is the superposition rule of the K:

$$K_{tot} = K_{app} + K_{res} \tag{A3}$$

Which, under the plane stress condition, can also be written as:

$$\sqrt{G_{tot}E} = \sqrt{G_{app}E} + \sqrt{G_{res}E} \tag{A4}$$

where $G_{tot} = \frac{1}{2t\Delta a} F_{tot} v_{tot}$, $G_{app} = \frac{1}{2t\Delta a} F_{app} v_{app}$ and $G_{res} = \frac{1}{2t\Delta a} F_{res} v_{res}$.

From eq. (A5), we have:

$$\sqrt{\left(F_{app} + F_{res}\right)\left(v_{res} + v_{app}\right)} = \sqrt{F_{res}v_{res}} + \sqrt{F_{app}v_{app}} \tag{A5}$$

Squaring both sides and simplify:

$$F_{res}v_{app} + F_{app}v_{res} = 2\sqrt{F_{app}v_{res}F_{res}v_{app}} \tag{A6}$$

Square both sides and simplify again:

$$(F_{res}v_{app})^2 + (F_{app}v_{res})^2 + 2F_{app}v_{res}F_{res}v_{app} = 4F_{app}v_{res}F_{res}v_{app} \tag{A7}$$

That is: $$(F_{res}v_{app} - F_{app}v_{res})^2 = 0 \tag{A8}$$

Therefore: $$F_{res}v_{app} = F_{app}v_{res} \tag{A9}$$

This is the Betti-Rayleigh reciprocal theorem that states that *in a linear elastic solid, the work done by a set of force acting through the corresponding displacements produced by a second set of forces is equal to the work done by the second set of forces acting through the corresponding displacements produced by the first set of forces* [29].

Hence the G_{tot} can be written as:

$$G_{tot} = \frac{1}{2t\Delta a}(F_{app}v_{app} + F_{res}v_{res} + 2F_{app}v_{res}) \tag{A10}$$

Thus:

$$G_{tot} = G_{app} + G_{res} + G_{mut} \neq G_{app} + G_{res} \tag{A11}$$

where $$G_{mut} = F_{app} v_{res} + F_{res} v_{app} = 2F_{app} v_{res} = 2F_{res} v_{app} \quad \text{(A12)}$$

Fig. 7 shows a numerical calculation to demonstrate the superposition of SIF in LEFM and of the G_{tot} to demonstrate that the mutual energy terms must be taken into account when superimposing the strain energy release rates due to different applied stresses.

References

1. Schmidt H-J, Voto C, Hansson J. TANGO metallic fuselage barrel validation of advanced technologies. In: Design for Durability in the Digital Age, Proc. 21st Symposium of the International Committee on Aeronautical Fatigue, ICAF 2001, Vol. 1, pp. 273-288, Ed. J. Rouchon, Pub. Cepadues-Editions.
2. Pettit RG, Wang JJ, Toh C. Validated feasibility study of integrally stiffened metallic fuselage panels for reducing manufacturing costs, NASA/CR-2000-209342, May 2000.
3. Ghidini T, Dalle Donne C. Fatigue crack propagation assessment based on residual stresses obtained through cut-compliance technique, Fatigue & Fracture of Engineering Materials and Structures, 30(2006): 214-222.
4. Bussu G, Irving PE. The role of residual stress and heat affected zone properties on fatigue crack propagation in friction stir welded 2024-T351 aluminium joints", International Journal of Fatigue, 25(2003): 77-88.
5. Edwards L, Fitzpatrick ME, Irving PE, Sinclair I, Zhang X, Yapp D. An integrated approach to the determination and consequences of residual stress on the fatigue performance of welded aircraft structures. ASTM International, Vol. 3, Feb 2006. Online ISSN: 1546-962X. Paper ID JAI12547; available online at www.astm.org.
6. Glinka G. Effect of residual stresses on fatigue crack growth in steel weldments under constant and variable amplitude load. In: Fract. Mech., ASTM STP 677, American Society for Testing and Materials, 1979, pp. 198-214.
7. Parker AP. Stress intensity factors, crack profiles, and fatigue crack growth rates in residual stress fields. In: Residual Stress Effects in Fatigue, ASTM STP 776, American Society for Testing and Materials, 1982, pp. 13-31.
8. Itoh YZ, Suruga S, Kashiwaya H. Prediction of fatigue crack growth rate in welding residual stress field, Eng Fract Mech, 33 (1989): 397-407.
9. Beghini M, Bertini L. Fatigue crack propagation through residual stress fields with closure phenomena", *Engineering Fracture Mechanics,* 36 (1990): 379-387.
10. Beghini M, Bertini L, Vitale E. Fatigue crack growth in residual stress fields: experimental results and modelling, *Fatigue & Fracture of Engineering Material & Structures,* 17(1994): 1433-1444.
11. Choi H-C, Song J-H. Finite element analysis of closure behaviour of fatigue cracks in residual stress fields, Fatigue & Fracture of Engineering Materials and Structures, 18(1995): 105-117.
12. Brouard J, Lin J, Irving PE. Effects of residual stress and fatigue crack closure during fatigue crack growth in welded 2024 aluminium. In : Proc. of Fatigue 2006, June 2006, Atlanta, USA.

13. Liljedahl CDM, Tan ML, Zanellato O, Ganguly S, Fitzpatrick ME, Edwards L. Evolution of residual stresses with fatigue loading and subsequent crack growth in a welded aluminium alloy middle tension specimen, *Eng Fract Mech,* 75 (2008): 3881-3894.

14. Pouget G, Reynolds AP. Residual stress and microstructure effects on fatigue crack growth in AA2025 friction stir welds, Int J Fatigue, 30(2008): 463-472.

15. Elber W. The significance of fatigue crack closure. Damage Tolerance in Aircraft Structures, ASTM STP 486, 1971: 230-242.

16. Glinka G, Shen G. Universal features of weight functions for cracks in mode I, Engineering Fracture Mechanics, 40 (1991): 1135-1146.

17. Walker K. The effect of the stress ratio during crack propagation and fatigue for 2024-T3 and 7075-T6 aluminium. *ASTM STP 462,* vol. 462, Effects of environment and complex load history on fatigue life, pp. 1-14.

18. Harter JA. AFGROW users guide and technical manual, AFRL-VA-WP-TR-2006-XXXX, AFGROW for Windows 2K/XP, Version 4.0011.14, June 2006. Website (accessed July 2008): http://www.siresearch.info/projects/afgrow/downloads/afgrow/ddownload.php.

19. Forman RG, Mettu SR. Behaviour of surface and corner cracks subjected to tensile and bending loads in Ti-6Al-4V alloy. Fracture Mechanics 22nd Symposium, Vol. 1, ASTM STP 1131, HA Ernst, A Saxena and DL McDowell eds., American Society for Testing and Materials, Philadelphia, 1992.

20. SAE Fatigue Design and Evaluation Committee. Fatigue Design Handbook, 3rd ed., Society of Automotive Engineers; 1997.

21. Noroozi AH, Glinka G, Lambert S. A study of the stress ratio effects on fatigue crack growth using the unified twp-parameter fatigue crack growth driving force, Int J Fatigue, 29 (2007): 1616-1633.

22. Noroozi AH, Glinka G, Lambert S. A two parameter driving force for fatigue crack growth analysis, Int J Fatigue, 27 (2005): 1277-1296.

23. ABAQUS user/technical manual version 6.5. Hibbit, Karlsson & Sorensen Inc.; 2005

24. Rybicki EF, Kanninen M.F. A finite element calculation of stress intensity factors by a modified crack closure integral. Eng Fract Mech, 9(1977): 931-938.

25. Anderson TL. Fracture Mechanics: Fundamentals and Applications. Third Edition. CRC Taylor & Francis. P. 60.

26. AFGROW computer code (version 4.11.14.0, 2006); accessed June 2008. http://www.siresearch.info/projects/afgrow/downloads/afgrow/ddownload.php.

27. Schijve, J. Some formulas for the crack opening stress level. Eng Fract Mechanics, 14(1981): 461-465.

28. Newman, JC Jr. A crack closure stress equation for fatigue crack growth. Int J of Fracture. 24(1984): R131-R135.

29. Fung, YC. Foundations of Solid Mechanics. Prentice-Hall, Inc. 1965. Page 5-6.

Tables

Table 1 Material constants used in the crack growth laws for 2024-T351*.

Walker eq.	$C = 4.80 \times 10^{-11}$	$n = 3.2$	$m = 0.6937$	
NASGRO eq.	$C = 1.71 \times 10^{-10}$	$n = 3.353$	$p = 0.5$	$q = 1$

* Data source: NASGRO database on 2024-T351 (plate & sheet; L-T) from the AFGROW computer code version 4.11.14.0 [26]. Units: da/dN and C in m/cycle, ΔK in MPa $m^{1/2}$

Table 2 Calculated R_{eff} and ΔK_{eff} for two constant amplitude load tests*.

a		$R = 0.1$	$\Delta\sigma = 46.4$			$R = 0.6$	$\Delta\sigma = 42.6$	
(mm)	ΔK_{app}	R_{eff}	U	ΔK_{eff}	ΔK_{app}	R_{eff}	U	ΔK_{eff}
5	5.93	0.62	0.75	4.34	5.37	0.76	0.80	4.31
7	7.08	0.64	0.76	5.24	6.41	0.77	0.81	5.17
10	8.63	0.61	0.74	6.28	7.82	0.75	0.80	6.26
12	9.44	0.67	0.77	7.23	8.72	0.78	0.81	7.08
15	10.93	0.70	0.78	8.53	10.09	0.80	0.82	8.27
17	11.97	0.70	0.78	9.33	11.06	0.80	0.82	9.05
20	13.68	0.67	0.77	10.53	12.64	0.78	0.81	10.28
22	14.97	0.64	0.75	11.29	13.83	0.77	0.81	11.15

* Units: $\Delta\sigma$ in MPa, ΔK in MPa$\sqrt{m}$.

Figures

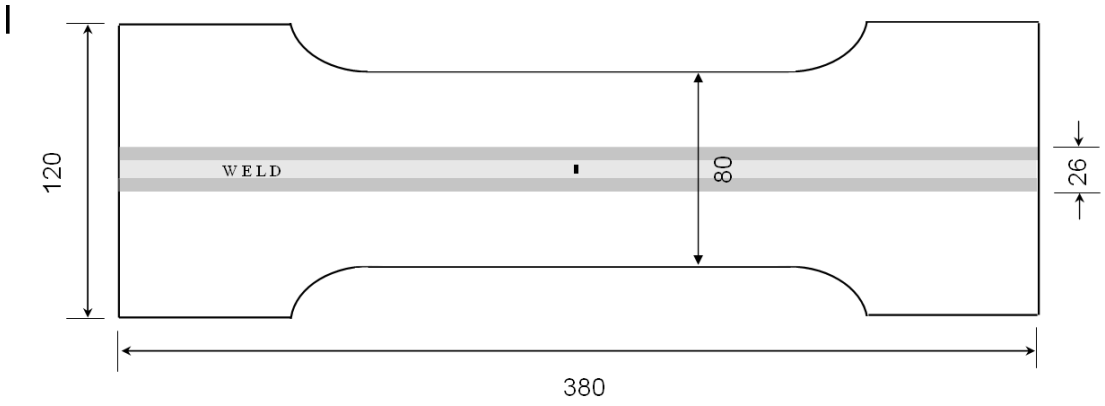

Fig. 1 M(T) specimen: dimension and weld position (thickness = 7; unit: mm) [13].

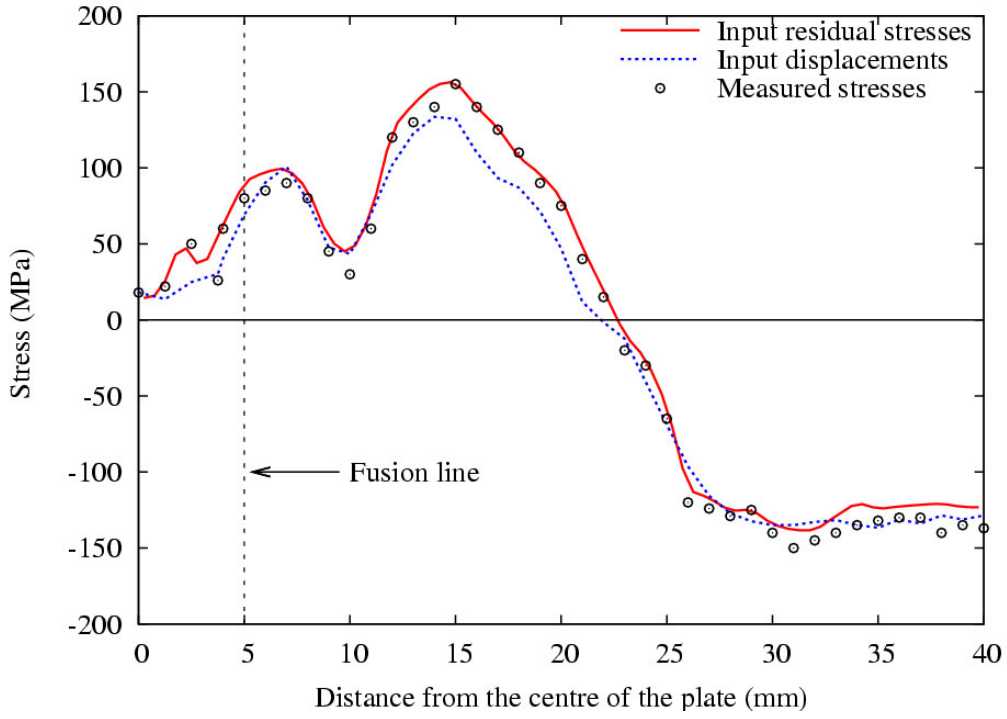

Fig. 2 Initial residual stress fields in the FE models by inputting either the measured stresses or equivalent displacements and comparison with measured data in [13].

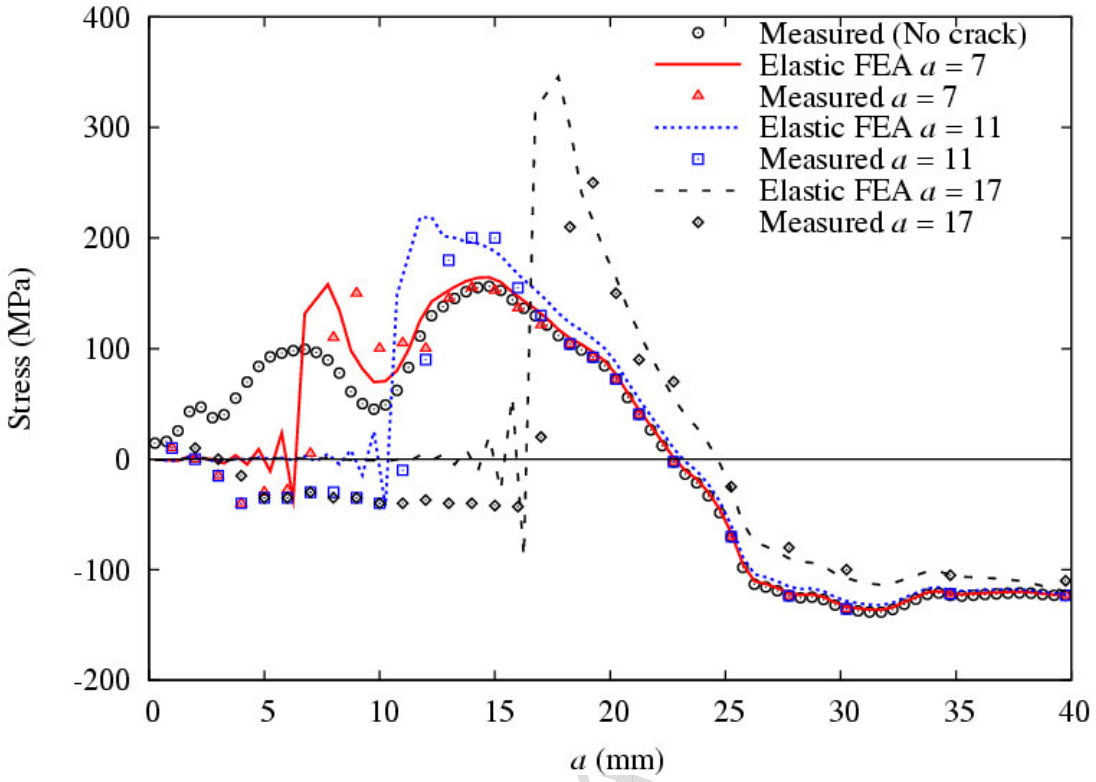

Fig. 3 Evolution of longitudinal residual stresses with crack extension: FE modelling results vs. measurement.

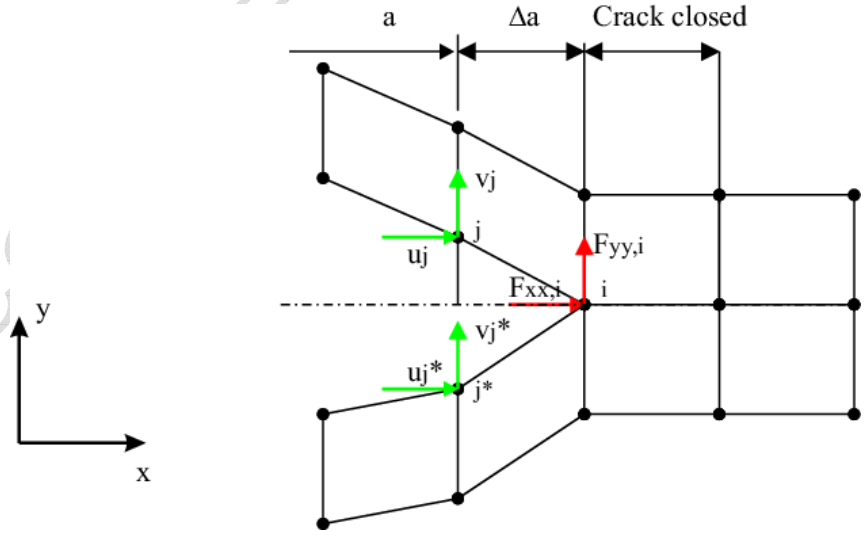

Fig. 4 Schematic of the MVCCT.

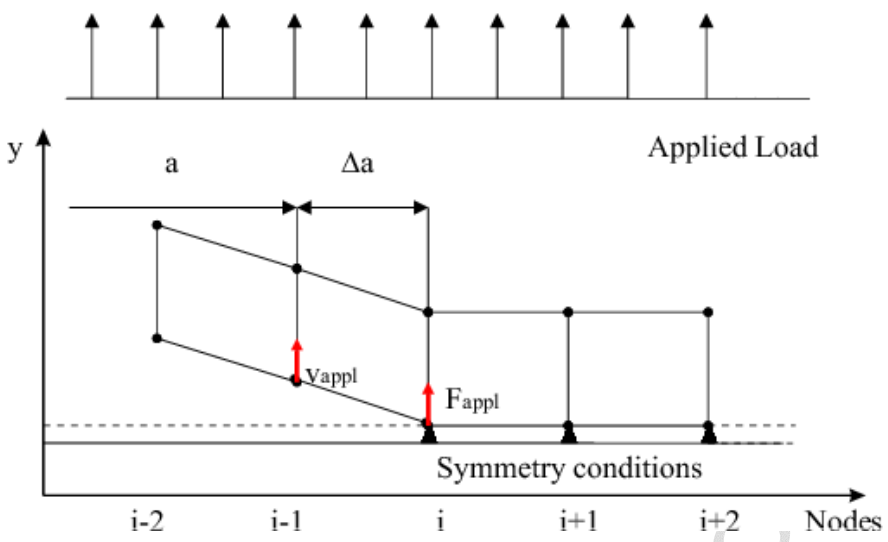

Fig. 5(a) Schematic of MVCCT under externally applied mechanical load (Showing only the top layer of the finite elements over crack surface).

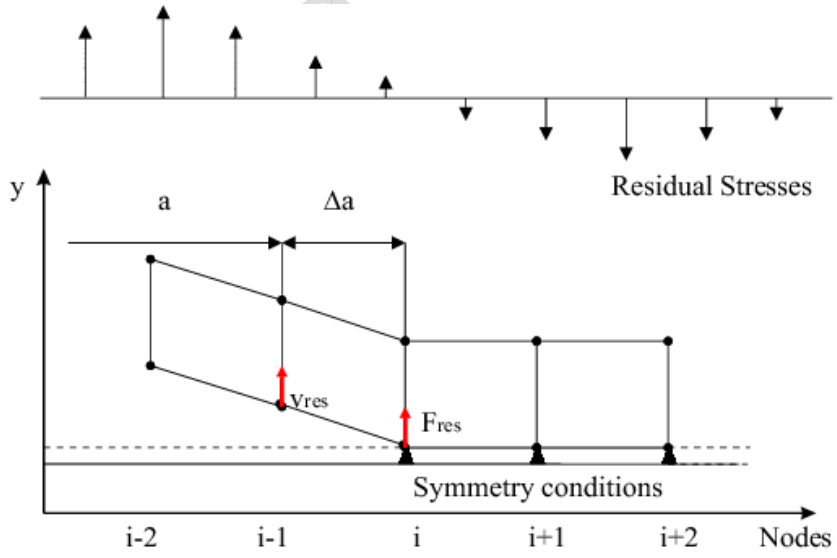

Fig. 5(b) Schematic of MVCCT subjected to internally balanced residual stress field (Showing only the top layer of the finite elements over crack surface).

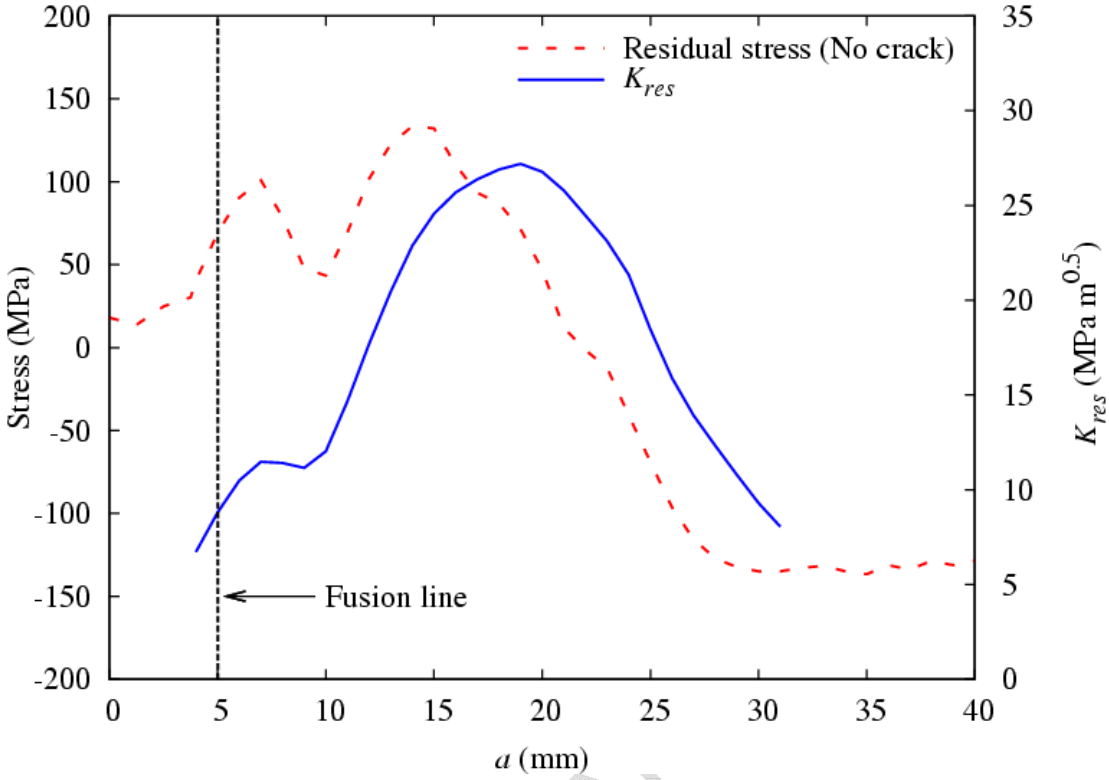

Fig. 6 Distribution of initial longitudinal residual stress and calculated K_{res}

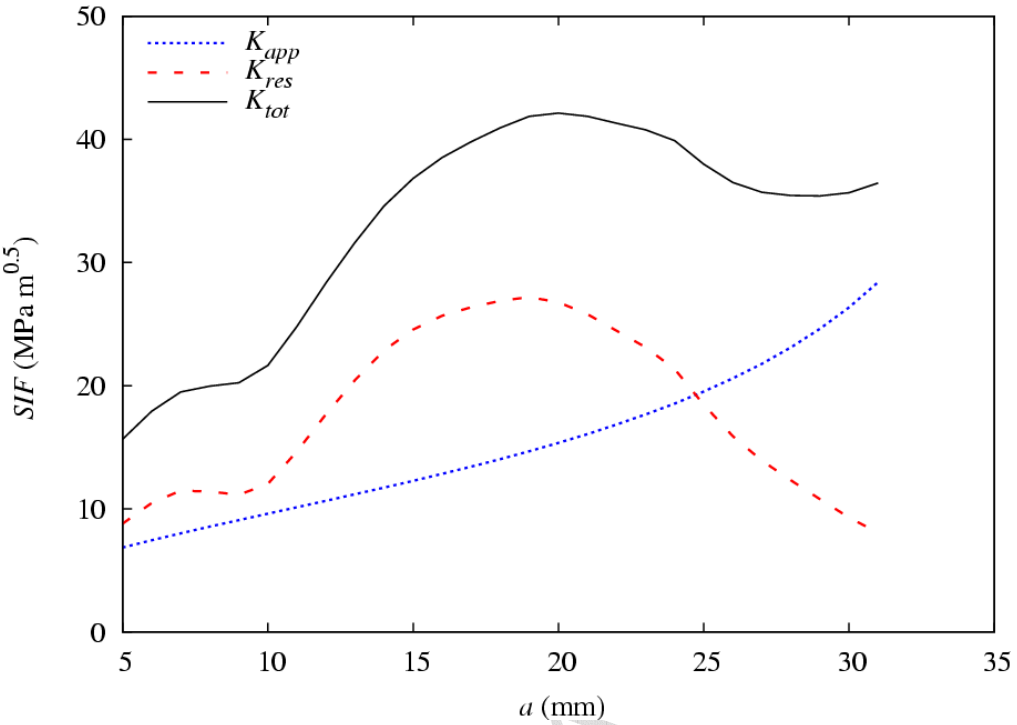

Fig. 7(a) Superposition of stress intensity factors (SIF); applied stress = 50 MPa.

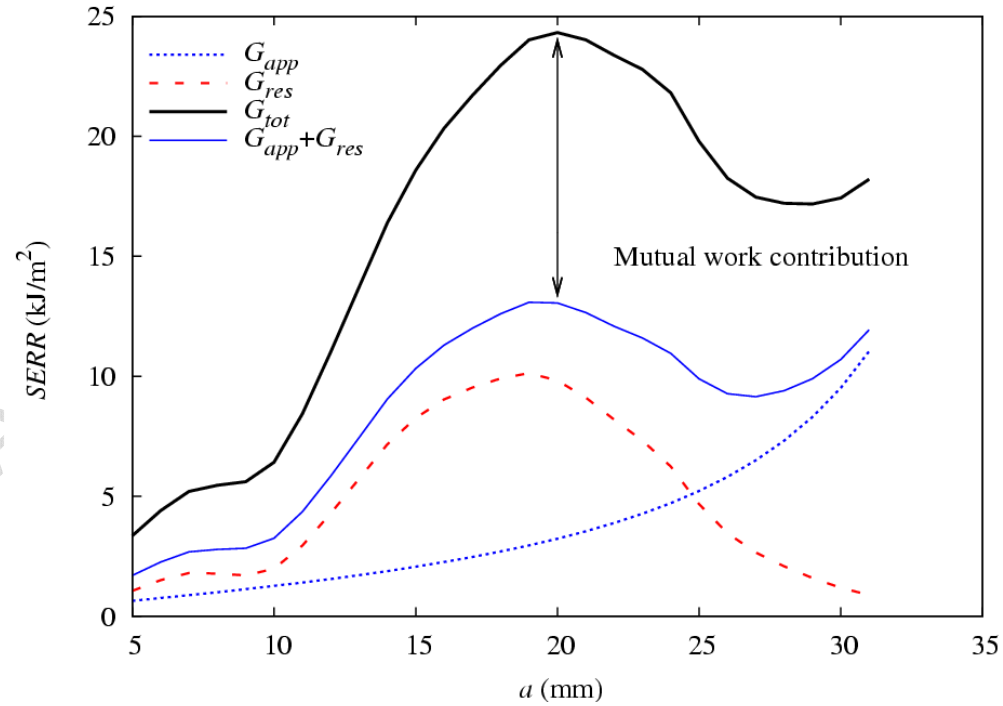

Fig. 7(b) Superposition of strain energy release rates (G_{app} + G_{res}) and comparioson with the G_{tot} that includes the mutual work; applied stress = 50 MPa

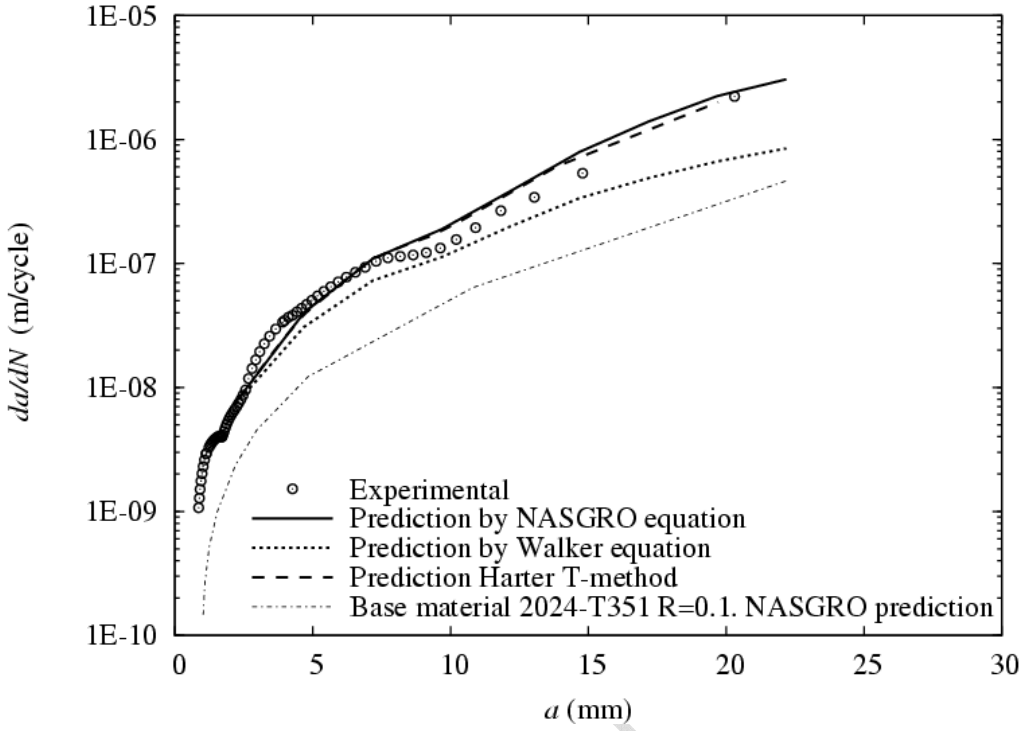

Fig. 8(a) Predicted and measured fatigue crack growth rates under constant amplitude load: $\Delta\sigma$= 46.4 MPa, R = 0.1.

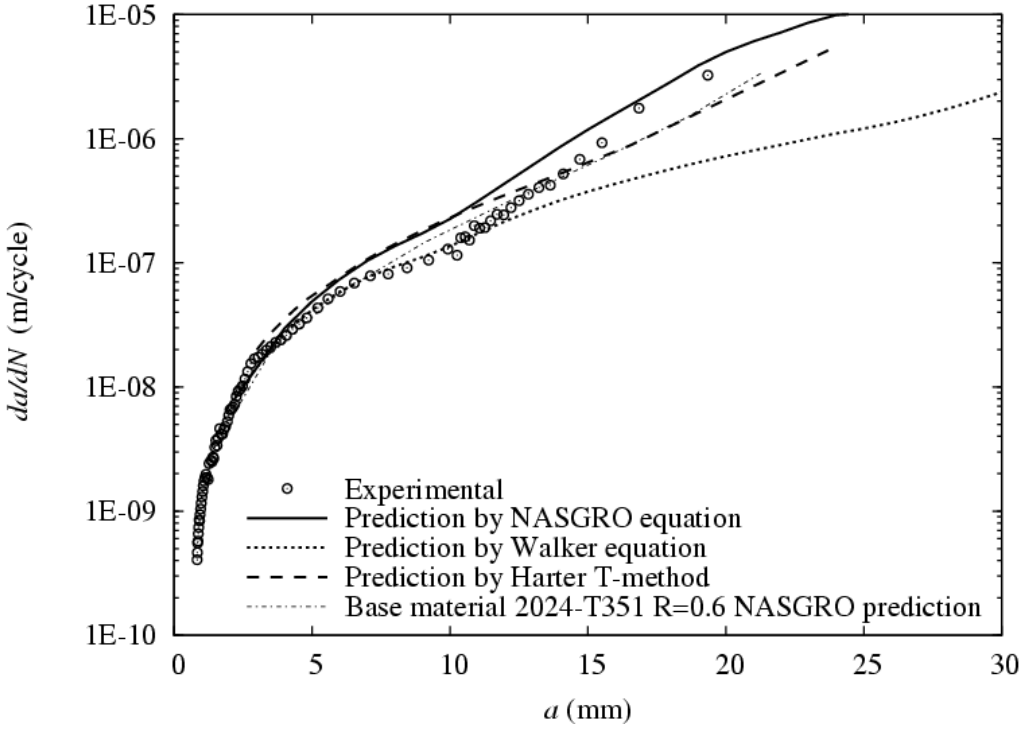

Fig. 8(b) Predicted and measured fatigue crack growth rates under constant amplitude load: $\Delta\sigma$= 42.6 MPa, R = 0.6

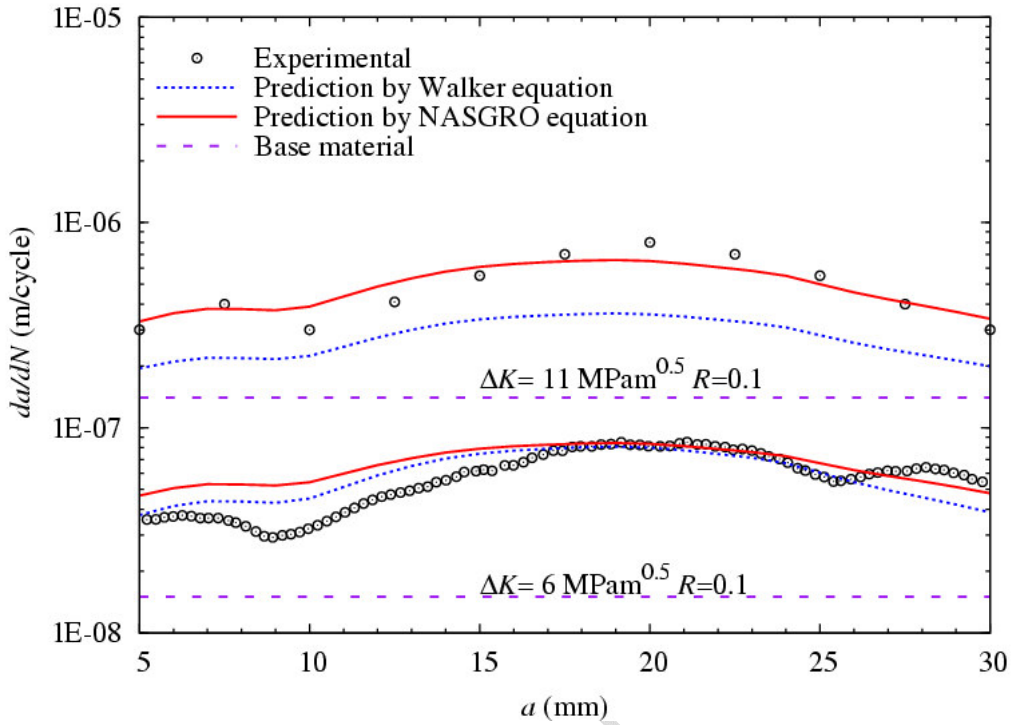

Fig. 9 Predicted and measured fatigue crack growth rates under constant SIF range: ΔK = 6 and 11 MPa √m.

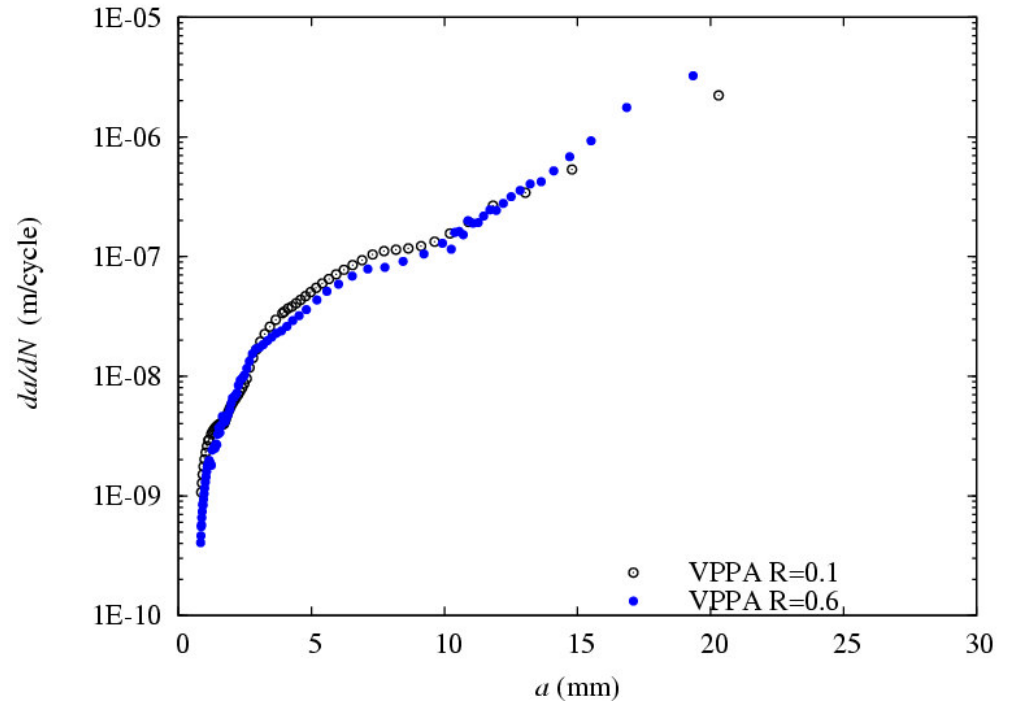

Fig. 10 Measured fatigue crack growth rates from experiments conducted in [12]; constant amplitude loads: $\Delta\sigma$ = 46.4 MPa, R = 0.1 and $\Delta\sigma$ = 42.6 MPa, R = 0.6.

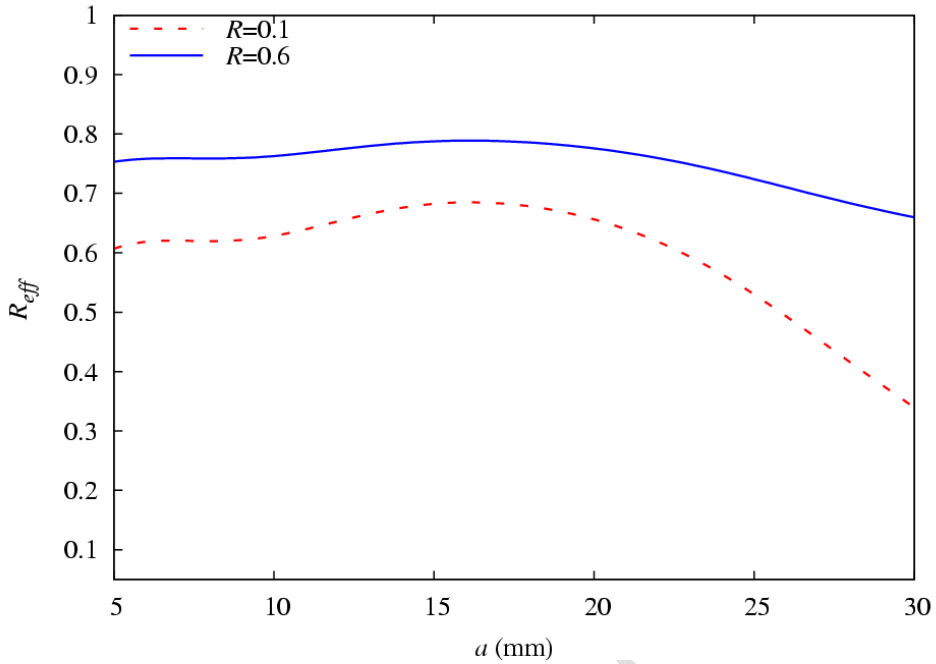

Fig. 11 Calculated effective stress ratios (R_{eff}) for nominal stress ratio R = 0.1, 0.6.

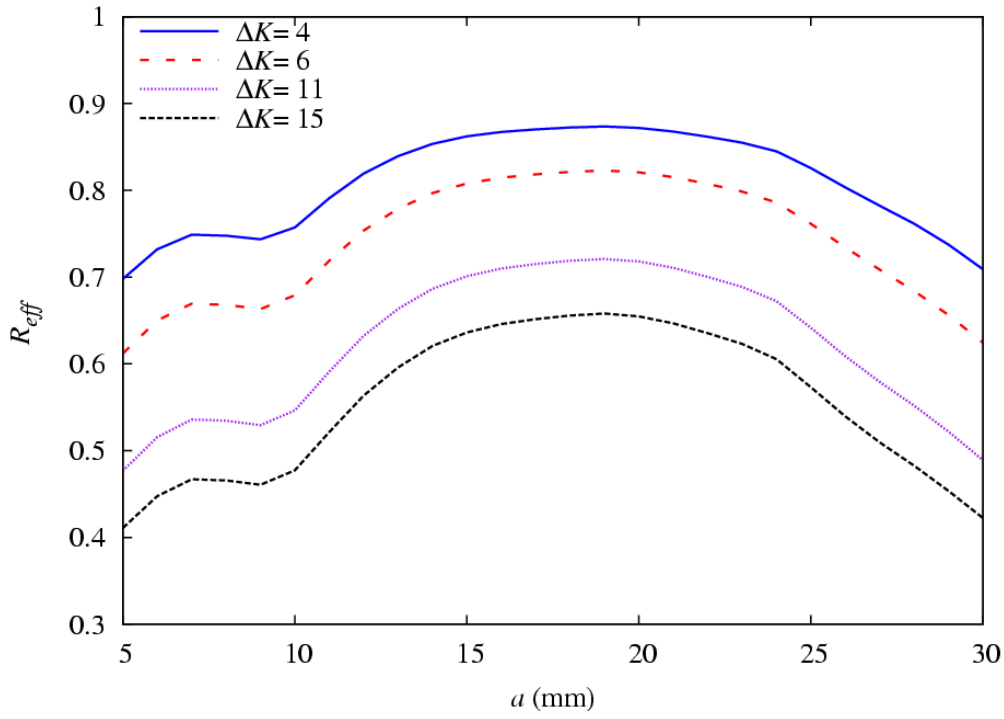

Fig. 12 Calculated effective stress ratios (R_{eff}) for different constant SIF ranges.